# Kinetics of Photoinduced Electron Transfer in Polythiophene−Porphyrin−Fullerene Molecular Films

**Tommi Vuorinen,* Kimmo Kaunisto, Vladimir Chukharev, Nikolai V. Tkachenko, Alexandre Efimov, and Helge Lemmetyinen**

*Institute of Materials Chemistry, Tampere University of Technology, P.O. Box 541, FIN-33101 Tampere, Finland*

*Received: May 19, 2006; In Final Form: July 24, 2006*

Photoinduced electron transfer (ET) processes were studied by the time-resolved Maxwell displacement charge (TRMDC) method in bilayer structures consisting of an electron donor−acceptor and conductive polymer monolayers, porphyrin−fullerene dyad and polyhexylthiophene, respectively, both layers prepared by the Langmuir−Blodgett (LB) method. The charge separation involves two fast steps: an intramolecular ET in the dyad molecule followed by an interlayer ET from the polymer to the formed porphyrin radical cation. These fast vertical intra- and interlayer processes could not be time-resolved by the TRMDC method. The lifetime of the charge separated state in the system was extended to hundreds of milliseconds by lateral electron and hole transfers in fullerene and polymer sublayers. The kinetics of the system was described by a model involving two long-living energetically different complete charge separated states. The data analysis indicates that the charge separation has a recombination time of 0.5 s. This is a promising result for possible applications.

## 1. Introduction

A quest for new organic photovoltaic materials has been a motivation for molecular design and engineering to build molecular electron donor−acceptor (DA) systems capable of photoinduced charge transfer reactions.[1−8] To convert light to electric energy, an efficient photoinduced charge separation is required. A fast photoinduced intramolecular electron transfer reaction can be achieved in covalently linked electron donor−acceptor dyads,[9−18] triads,[19−27] and tetrads.[28,29] To utilize the charge separated state, one can try to organize the dyads as molecular films, for example, by means of the Langmuir−Blodgett (LB) technique[30−35] or the self-assembly method.[5−8,36] In a molecular photovoltaic device, the separated charges have to be evacuated quickly from the donor and acceptor radical ions through electrodes to an external circuit to avoid losses due to the charge recombination. This requires a molecular device composed of at least three functional layers, all of which have to fulfill their own task:[32,37] the fast primary photoinduced charge separation has to take place in the donor−acceptor layer, and the hole and electron transport layers have to capture the respective charges from the radical ions formed and transfer them to the electrodes.

Previously, we have utilized the time-resolved Maxwell displacement charge (TRMDC) method to study vectorial photoinduced charge transfer in LB films of donor−acceptor dyads.[30,31,33] We have also shown that the charge separation time in the dyad LB monolayer can be extended by a secondary electron donation from polyhexylthiophene (PHT) to the donor cation.[32,37,38] The secondary electron transfer from PHT to the porphyrin cation corresponds to the above-discussed hole capture and transport in the molecular photocell.

The charge transfer process involves forward and backward reactions, the charge separation and the charge recombination, respectively. In this study, in a solid phase electron transfer system, when excited with continuous light, both the photoinduced charge separation and spontaneous recombination reactions are taking place simultaneously and finally equilibrium between the processes is reached. The time-resolved Maxwell displacement charge (TRMDC) method applied in the photocurrent mode provides a tool for monitoring electron transfer kinetics in organized molecular film systems under the continuous photoexcitation. This work proposes a kinetic model for transient photocurrent measurements to determine the charge recombination rate constants in the supramolecular triad systems.

## 2. Experimental Section

**2.1. Materials.** Chloroform of analytical grade (Merck) was used for solution preparation and spreading solvent without any further purification. The matrix molecule for the LB film, octadecylamine (ODA), was of 99% grade (Sigma). The synthesis for the studied porphyrin−fullerene dyads, DHD6ee and ZnDHD6ee, is described elsewhere.[39] Regioregular poly(3-hexylthiophene) (PHT) was purchased from Aldrich and was of 98.5% grade. The structures for the photoactive materials utilized are presented in Figure 1. The chloroform solutions were prepared to have concentrations of 1 mg $mL^{-1}$ for dyad and ODA and 0.2 mg $mL^{-1}$ for PHT. The spreading solutions were diluted from these stock solutions to total concentrations equal or less than 1.0 mM.

**2.2. Film Preparations.** The LB 5000 and LB 2000 systems (KSV Instruments, Helsinki, Finland) were used for the isotherm measurements and the film depositions. The subphase was a phosphate buffer containing 0.5 mM $Na_2HPO_4$ and 0.1 mM $NaH_2PO_4$ (pH ∼ 7) in ion-exchanged Milli-Q water. The subphase temperature was adjusted with a thermostat to 18 ± 0.5 °C. Films for spectroscopic measurements were deposited

* To whom correspondence should be addressed. E-mail: tommi.vuorinen@tut.fi. Phone: +358-3-3115-3629. Fax: +358-3-3115-2108.

10.1021/jp063076b CCC: $33.50 
Published on Web 09/02/2006

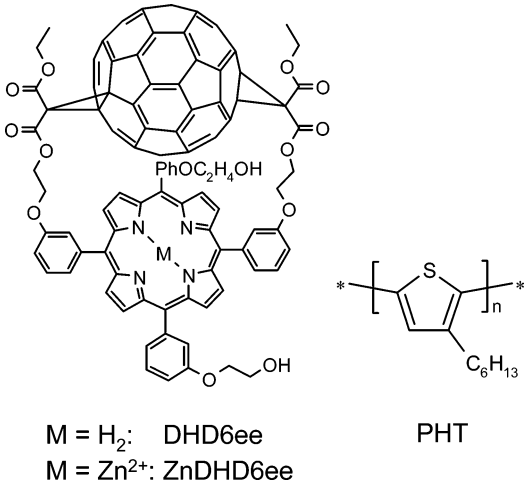


**Figure 1.** Structures for DHD6ee, ZnDHD6ee, and PHT.

onto quartz substrates cleaned with a standard procedure[40] and plasma etched prior to use for 15 min in a low-pressure nitrogen atmosphere with plasma cleaner PDC-23G (Harrick). For the photoelectrical measurements, glass slides covered by semi-transparent ITO (indium tin oxide) electrode were cleaned in an ultrasonic bath first in acetone and then in chloroform and plasma etched in nitrogen for 10 min prior to use. Half of the area of the ITO electrodes was removed by treatment with acid.[37]

The film formation and deposition conditions for the dyads are described in detail elsewhere.[33] In this work, the dyad concentrations in the LB film preparations were 10 and 18 mol % in ODA for DHD6ee and ZnDHD6ee, respectively. The dyad monolayer deposition was done at a surface pressure of 15 mN $m^{-1}$ with deposition rates of 5 mm $min^{-1}$ in both directions. PHT was mixed with ODA in a concentration of 60 mol %, counted per PHT monomer unit. The PHT deposition pressure was 20 mN $m^{-1}$, and the rates were 4 and 7 mm $min^{-1}$ for the air-to-water and water-to-air directions, respectively.[38] The deposition directions water-to-air and air-to-water are designated in this paper as up and down, respectively.

A general structure of the sample for electrical measurements was ITO|insulating ODA layers|active layers|insulating ODA layers|Al top electrode. The 50 nm thick aluminum electrodes were thermally evaporated through a mask onto the LB layers in high vacuum ($p < 10^{-5}$ mbar) with a BOC Edwards Auto 306 coating system.[37] The Al electrodes had approximately 1 $mm^2$ overlapping area with the ITO electrode. The exact areas were determined for individual electrodes in each measurement.

**2.3. Absorption Measurements.** The absorption spectra of the LB films were recorded by a Shimadzu UV-2501 PC spectrophotometer.

**2.4. Electrical Measurements.** The electron donor−acceptor dyad molecules can be ordered, for example, by the LB method, to have the same mutual orientation throughout the whole film structure. Because of the orientation of the DA pairs, the electron transfer occurs vectorially always in the same direction everywhere in the film. The TRMDC method can be used to measure the charge movements inside thin films causing an electrical component in the direction perpendicular to the electrode planes,[30,31,41] but the charge movements with the electrical component parallel to the electrode plane do not produce electrical signals. The TRMDC measurement circuit and the sample structure were similar to those reported previously (see Scheme 2 in ref 37). Since the photoactive layers are insulated from the electrodes, the photoinduced TRMDC signals are caused by the charges induced on the electrodes by the electron movements inside the active layers perpendicular to the film plane. The films between the electrodes have very low conductivity ($R_s > 10^{12}$ Ω), and therefore, the system can be treated as a capacitor with a typical capacitance, $C_s$, of approximately 300 pF. During the measurements, a preamplifier with a 100 MΩ input resistance ($R_{in}$) was used.

**TABLE 1: Parameters for Calculation of the Bilayer Absorption Cross Sections, $\sigma$, at the Excitation Band[a]**

| bilayer | $\eta_{exc}$ | $A$ | $n$, $\times 10^{13}$ cm$^{-2}$ | $\sigma$, $\times 10^{-16}$ cm$^2$ |
|---|---|---|---|---|
| PHT−DHD6ee | 0.81 | 0.026 | 3.0 | 7.1 |
| PHT−ZnDHD6ee | 0.68 | 0.030 | 4.7 | 4.4 |

[a] $\eta_{exc}$ is the spectral overlap of the bilayer absorption and excitation light bands, $A$ is the fraction of absorbed light at the Soret band, and $n$ is the number density of the dyad.

The TRMDC measurements can be carried out in a photovoltage (PV) mode or in a photocurrent (PC) mode. The essential difference between the modes is their time domain. The time limit between the modes is an instrumental time constant, $\tau_{RC} = R_{in}C_s$. The PV signals are recorded in a time domain much shorter than $\tau_{RC}$. Thus, discharge of the capacitor $C_s$ over loading resistance $R_{in}$ is negligible and the measured signal is essentially the potential at $C_s$. The photovoltage response amplitude is proportional to the charge separation distance and to the number of electrons.[41] In the PC mode, the time domain used is much longer than $\tau_{RC}$; therefore, the voltage over the sample is virtually zero and the measured signal is essentially the current through the amplifier input resistor, $R_{in}$. The measured transient photocurrent is proportional to the rate of change of concentration of the charge separated states in the film.[41] In the photocurrent mode, the TRMDC method time resolution is limited by $\tau_{RC}$.

The photovoltage signals were created by a 10 ns laser pulse excitation. After the excitation, the change of the potential was followed with time. In the PC mode, the films were excited by the continuous light of an arc lamp and the transient photocurrent signals were recorded with a Tektronix 2212 digital oscilloscope. The excitation wavelength for the PC measurements was selected by a monochromator or a set of color filters. The maximum transmission of the color filter set was at 430 nm with a bandwidth of approximately 30 nm, and the maximum excitation power density was 5 mW $cm^{-2}$. The excitation light densities were adjusted with neutral density filters.

## 3. Results and Discussion

**3.1. UV−vis Absorption.** An average bilayer (dyad + polymer) absorption cross section, $\sigma$, at the excitation light band can be presented with an equation

$$\sigma = -\ln(1 - \eta_{exc}A)/n \qquad (1)$$

where $\eta_{exc}$ is the spectral overlap of the absorption and excitation bands, $A$ is the fraction of the absorbed light at the Soret band (435 ± 5 nm) of the porphyrin molecule, and $n$ is the number density of the dyad molecules in the monolayer determined by measuring the surface pressure−area isotherm.[33] The values for the parameters are presented in Table 1 together with the calculated cross sections.

**3.2. TRMDC Measurements.** The photoinduced electron transfer in the DHD6ee and ZnDHD6ee LB monolayers has been studied by the TRMDC method in the PV mode.[33] In the present study, the PHT and dyad monolayers were deposited consecutively in such a way that the polymer was in direct contact with the porphyrin moiety of the dyad. The PHT−

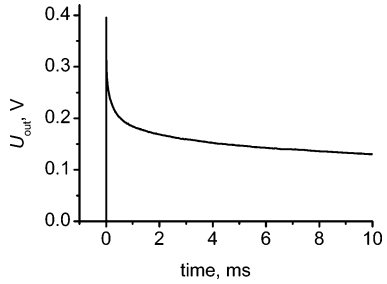


**Figure 2.** Photovoltage response signal for the PHT−ZnDHD6ee bilayer. The PV response signal was recorded with a preamplifier input resistance, $R_{in}$, of 1 GΩ.

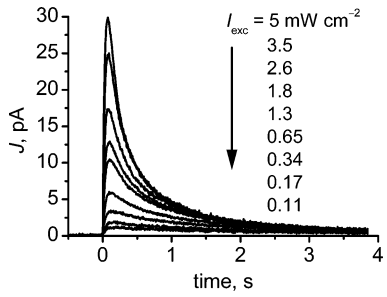


**Figure 3.** Photocurrent response signals for a bilayer sample with structure ITO|ODA|ZnDHD6ee (down)|PHT (up)|ODA|Al. The excitation intensity varied from 0.11 to 5 mW cm$^{-2}$.

DHD6ee bilayer showed a 3.5-fold photovoltage amplitude compared to that of the dyad monolayer.[37] Since the PV amplitude is proportional to the charge separation distance,[41] the increase in the PV amplitude can be explained by a two-step electron transfer process: the primary electron transfer occurs intramolecularly from porphyrin to fullerene followed by the secondary electron transfer from PHT to the porphyrin radical cation formed in the first step. The charge separation distance in the dyad monolayer is estimated to be 0.5 nm.[33] One can consider that the PHT film provides an average increase of 1.5 nm in the electron transfer distance taking into account the fact that the polymer layer thickness is about 3 nm.[42] Thus, the 3.5-fold increase in the PV amplitude can be attributed to the increased charge separation distance by the PHT film. The time resolution of the instrument in the PV mode is 20 ns. In solutions, the formation of the charge separated state in the dyad takes place in tens of picoseconds.[43] Thus, the actual charge separations in the dyad and the interlayer electron transfer (ET) from PHT to the porphyrin cation are too fast to be time-resolved in the electrical measurements.

The photovoltage measurement (Figure 2) shows that the charge recombination in the PHT−dyad bilayer is not yet completed after 10 ms. The upper limit for the PV measurements is approximately 10 ms with $R_{in} = 100$ MΩ. To determine the charge recombination kinetics in longer time scales and thus estimate the recombination times, one can carry out the TRMDC measurements in the photocurrent mode. Previously, we have treated the PC results with the simplest possible scheme containing a ground state, an excited state, and a charge separated state.[37] This scheme yields a monoexponential decay for the PC signal. Closer examination of the results suggests that a sum of two exponentials is needed to fit the decay of the transient photocurrent. Thus, a function, $J(t) = \sum a_i \exp[t/\tau_i]$, with three exponentials was applied to fit the photocurrent response signals (Figure 3), where the first exponential corresponds to the instrumental $\tau_{RC}$, responsible for the rise of the signal, and the other two correspond to the decay of the measured current. The signals were measured at different

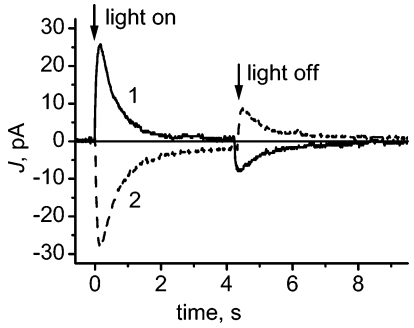


**Figure 4.** Transient photocurrent measured in the light on/off mode for a complementary bilayer film pair with the structures (1) ITO|ODA|DHD6ee (down)|PHT (up)|ODA|Al (solid line) and (2) ITO|ODA|PHT (down)|DHD6ee (up)|ODA|Al (dashed line).

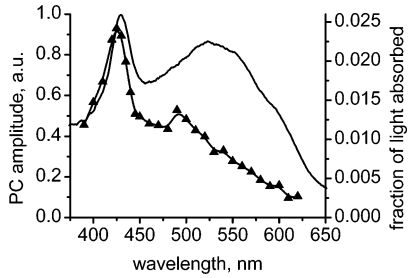


**Figure 5.** Photocurrent action spectrum for the bilayer PHT (down)/DHD6ee (up) shown with triangles. The absorption spectrum for the PHT−DHD6ee bilayer is shown with a solid line.

excitation power densities (Figure 3). The obtained values for the signal rise time are always close to the instrumental time constants, $\tau_{RC} \sim 30$ ms.

Under the continuous photoexcitation, the photoinduced charge separation takes place simultaneously with the spontaneous charge recombination back to the ground state. In the film structures used in this study, the insulating ODA layers prevent the charge transport from the active layers to the electrodes and thus no static current can flow through the film. Due to the slow recombination and to the blocked charge evacuation, the charge separated state of the whole system accumulates under continuous excitation. This leads up to a decrease in the population on the ground state and therefore the rate of the charge separation reaction, and the observed current decrease (Figures 3 and 4). Finally, an equilibrium between the charge separated and ground states is reached when the rates of the photoinduced charge separation and the spontaneous charge recombination become equal to each other. The equilibration causes the transient photocurrent to decay to zero (Figures 3 and 4). The constant excitation keeps up the equilibrium, but when the light is switched off, the equilibrium is broken and an opposite transient current due to the charge recombination can be seen (Figure 4). When the films were deposited in the opposite direction, that is, the bilayer structure was reversed, the polarity of the response signal was inverted, as seen in Figure 4. This proves that the direction of electron transfer in the bilayer structure is controlled by mutual orientations of the DA dyad and PHT layers as it was controlled by the dyad in the case of the dyad monolayers.[33]

To determine the photocurrent action spectra, the PC responses were recorded at various excitation wavelengths for the complementary PHT−DHD6ee bilayers. The obtained maximum current values were corrected with the power spectrum of the excitation source to calculate the action spectra (Figure 5). The photocurrent action spectra have well pronounced Soret bands, but in the range 500−600 nm, the photocurrent spectra

**SCHEME 1**

$$D_2\text{–}D_1\text{–}A \underset{k_4}{\overset{k_1}{\rightleftharpoons}} D_2^{+}\text{–}D_1\text{–}A^{-} \underset{k_3}{\overset{k_2}{\rightleftharpoons}} D'_2{}^{+}\text{–}D_1\text{–}A'^{-}$$

do not coincide with the PHT absorption band, showing a smaller contribution of PHT on the PC response. One can conclude that the vectorial photoinduced electron transfer in the bilayer structure results from the primary electron transfer from excited porphyrin to fullerene followed by the secondary electron transfer from PHT to the porphyrin cation. The low PC amplitude in the range 500−600 nm, compared to the PHT absorption, suggests that the direct electron transfer from PHT to fullerene is less probable.

**3.3. System Modeling.** Since the photocurrent time resolution is limited by $\tau_{RC}$, the fast primary intra- and secondary intermolecular electron transfer processes in the bilayer films cannot be time-resolved. By modeling the system at slow time domains, the charge separation processes can be reduced to the formation of long-living charge separated states. Thus, the PC measurements can be analyzed by using a scheme containing photoinduced transitions directly from the ground state to the final charge separated states (Scheme 1), where the negative and positive charges are located in the fullerene sublayer and the PHT layer, respectively. The negative and positive charges are supposed to migrate laterally in the respective layers.[38] In Scheme 1, A, $D_1$, and $D_2$ refer to the fullerene and porphyrin sublayers and the PHT layer, respectively. The model involves a ground state (GS), $D_2$−$D_1$−A, and two complete charge separated states with different energetic statuses, $D_2^{+}$−$D_1$−$A^{-}$ and $D'_2{}^{+}$−$D_1$−$A'^{-}$, referred to as $CS_1$ and $CS_2$, respectively. The $CS_1$ state is a polaron like state where negative and positive charges are aligned with the normal of the film plane. Transition from the ground state to the $CS_1$ state takes place with a rate constant, $k_1$, which can be given as a function of excitation power density, $I_{exc}$, as $k_1 = \sigma\phi I_{exc}$, where $\sigma$ is the absorption cross section at the excitation band and $\phi$ is the quantum yield for the interlayer ET in the formation of the $CS_1$ state. The $CS_2$ state is formed with rate $k_2$, when the charge moves from the donor or acceptor radical ion to neighboring site and polaron dissociates. Transitions between the $CS_1$ and $CS_2$ states describe the polaron dissociation and reassociation. The charge recombination back to the ground state can take place with rate constant $k_4$ only through the $CS_1$ state due to the vertical position and shorter distance between the electron and hole than in the $CS_2$ state. Similar lateral charge migration has been reported to take place in the viologen−perylene−ferrocene triad LB films.[44]

The differential rate equations for the states in Scheme 1 are

$$\begin{cases} \dfrac{dGS}{dt} = -k_1 GS + k_4 CS_1 \\ \dfrac{dCS_1}{dt} = k_1 GS - (k_2 + k_4) CS_1 + k_3 CS_2 \\ \dfrac{dCS_2}{dt} = k_2 CS_1 - k_3 CS_2 \end{cases} \quad (2)$$

where GS, $CS_1$, and $CS_2$ refer to the concentrations of the states. By using a vector notation, $\mathbf{x} = [GS\ CS_1\ CS_2]^T$, one can express eq 2 as

$$\frac{d\mathbf{x}}{dt} = \mathbf{K}\mathbf{x} \quad (3)$$

where the characteristic matrix is

$$\mathbf{K} = \begin{bmatrix} -k_1 & k_4 & 0 \\ k_1 & -k_2 - k_4 & k_3 \\ 0 & k_2 & -k_3 \end{bmatrix} \quad (4)$$

By substituting a trial solution, $\mathbf{x}(t) = \mathbf{v}\exp[\lambda t]$, where $\mathbf{v}$ is a constant vector, into eq 3, one finds that

$$\mathbf{K}\mathbf{x} = \frac{d\mathbf{x}(t)}{dt} = \lambda\mathbf{v}\exp[\lambda t] = \mathbf{K}\mathbf{v}\exp[\lambda t] \quad (5)$$

and $\lambda\mathbf{v} = \mathbf{K}\mathbf{v}$. Thus, $\mathbf{x}(t) = \mathbf{v}\exp[\lambda t]$ is a solution of eq 3 if $\lambda$ is an eigenvalue of $\mathbf{K}$ and $\mathbf{v}$ is a corresponding eigenvector. The general solution is the linear combination of the linearly independent solutions

$$\mathbf{x}(t) = c_1\mathbf{v}\exp[\lambda_1 t] + c_2\mathbf{v}\exp[\lambda_2 t] + c_3\mathbf{v}\exp[\lambda_3 t] \quad (6)$$

The eigenvalues of matrix $\mathbf{K}$ for Scheme 1 are

$$\begin{cases} \lambda_1 = -\dfrac{k_s + k_1 + k_2 + k_3 + k_4}{2} \\ \lambda_2 = \dfrac{k_s - k_1 - k_2 - k_3 - k_4}{2} \\ \lambda_3 = 0 \end{cases} \quad (7)$$

where $k_s = [k_4^2 + 2k_4(k_2 - k_3) + (k_2 + k_3)^2 + 2(k_4 - k_3 - k_2)k_1 + k_1^2]^{1/2}$. Since the observed time constants are related to the eigenvalues, $\tau_i^{-1} = -\lambda_i$, one can note two useful relations:

$$-(\lambda_1 + \lambda_2) = \tau_1^{-1} + \tau_2^{-1} = k_1 + k_2 + k_3 + k_4 \quad (8a)$$

$$(\lambda_2 - \lambda_1)^2 = (\tau_1^{-1} - \tau_2^{-1})^2 = k_s^2 \quad (8b)$$

One must set initial conditions in order to find a particular solution for the differential equations. When the light is just switched on at time $t = 0$, all molecules are in the ground state, and one can write $GS(0) = 1$ and $CS_1(0) = CS_2(0) = 0$. From these conditions with eq 6, one obtains values for constants $c_i$.

When taken into account that the rate constant $k_1$ is proportional to the excitation power density, $k_1 = \sigma\phi I_{exc}$, one obtains from eqs 8a and b the following relations:

$$\tau_1^{-1} + \tau_2^{-1} = \sigma\phi I_{exc} + k_2 + k_3 + k_4 \quad (9a)$$

$$(\tau_1^{-1} - \tau_2^{-1})^2 = A + BI_{exc} + CI_{exc}^2 \quad (9b)$$

where $A = k_4^2 + 2k_4(k_2 - k_3) + (k_2 + k_3)^2$, $B = 2\sigma\phi(k_4 - k_3 - k_2)$, and $C = (\sigma\phi)^2$. Thus, when $\tau_1^{-1} + \tau_2^{-1}$ and $(\tau_1^{-1} - \tau_2^{-1})^2$ are plotted as functions of excitation power density, linear and parabolic fits are applied, respectively. From the obtained parameters, one can calculate values for the charge separation quantum yield, $\phi$, and the rate constants $k_2$, $k_3$, and $k_4$. The transient photocurrent signals measured at the three lowest excitation densities were discarded in the analysis due to their low signal-to-noise ratios.

Figure 6 shows the linear and parabolic fits according to eqs 9a and b for the film structure ITO|ODA|ZnDHD6ee (down)|PHT (up)|ODA|Al. The obtained parameter values from the linear and parabolic fits for all of the film structures are listed in Table 2. For the parabolic fit, the constant $C$ was fixed with the $\sigma\phi$ value obtained from the corresponding linear fit. The values for the quantum yields and the rate constants calculated from the fit results are presented in Table 3.

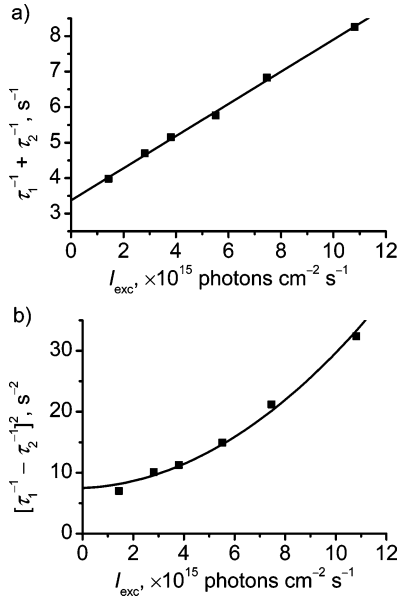


**Figure 6.** Analysis of obtained time constants $\tau_1$ and $\tau_2$ with (a) eq 9a and (b) eq 9b for the sample with structure ITO|ODA|ZnDHD6ee (down)|PHT (up)|ODA|Al.

**TABLE 2: Obtained Parameters from the Fits with eqs 9a and b[a]**

| film | $\sigma\phi$, ×10$^{-16}$ cm$^2$ | $k_2 + k_3 + k_4$, s$^{-1}$ | $A$, s$^{-2}$ | $B$, ×10$^{-16}$ cm$^2$ s$^{-1}$ |
|---|---|---|---|---|
| ITO−F−P−PHT | 3.84 | 4.14 | 11.90 | 4.83 |
| ITO−PHT−P−F | 3.47 | 3.96 | 10.70 | 4.15 |
| ITO−F−ZnP−PHT | 4.53 | 3.37 | 7.49 | 1.60 |
| ITO−PHT−ZnP−F | 1.63 | 3.33 | 5.49 | 1.76 |

[a] F refers to fullerene and P to porphyrin.

**TABLE 3: Charge Separation Quantum Yields and Rate Constants for Different Film Structures[a]**

| film | $\phi$ | $k_2$, s$^{-1}$ | $k_3$, s$^{-1}$ | $k_4$, s$^{-1}$ |
|---|---|---|---|---|
| ITO−F−P−PHT | 0.54 | 1.20 | 0.55 | 2.40 |
| ITO−PHT−P−F | 0.49 | 1.10 | 0.43 | 2.30 |
| ITO−F−ZnP−PHT | 1.00 | 1.10 | 0.77 | 1.80 |
| ITO−PHT−ZnP−F | 0.37 | 0.67 | 0.72 | 1.90 |

[a] F refers to fullerene and P to porphyrin.

To observe the kinetics in the dark, the transient photocurrent was recorded also in light on/off mode (Figure 4) with an excitation density of 5 mW cm$^{-2}$. Light was switched off when the transient current under light illumination had decayed close to zero and the equilibrium state was reached. In the dark, the response signal has the opposite polarity from that under photoexcitation because of the electron back transfer from the equilibrated CS states to the ground state. The charge recombination obeys Scheme 1 with rate constant $k_1 = 0$. The kinetics for the charge recombination can be treated in a similar way as for the photogeneration in eqs 2−7. The eigenvalues for the **K** matrix of charge recombination are

$$\begin{cases} \lambda_1 = -\dfrac{k_t + k_2 + k_3 + k_4}{2} \\ \lambda_2 = \dfrac{k_t - k_2 - k_3 - k_4}{2} \\ \lambda_3 = 0 \end{cases} \qquad (10)$$

where $k_t = [k_4^2 + 2k_4(k_2 - k_3) + k_3^2 + 2k_2k_3 + k_2^2]^{1/2}$. The charge recombination gives also a two-exponential decay of transient current with time constants of $\tau_i = -\lambda_i^{-1}$. The calculated sums of inversed time constants (eq 8a) for different bilayers are given in Table 4. The sum values are smaller for the reactions in the dark than those under illumination, since in the dark the rate constant $k_1$ is equal to zero. The sums of the rate constants differ from those obtained in excitation density dependence measurements due to the lower accuracy of the PC measurements in the on/off mode. However, the results of the on/off measurements support Scheme 1 for the studied systems.

**TABLE 4: Sums of the Inversed Decay Time Constants for Transient Photocurrents Measured in Light On/Off Mode[a]**

| | $\tau_1^{-1} + \tau_2^{-1}$, s$^{-1}$ | |
|---|---|---|
| film | light on | light off |
| ITO−F−P−PHT | 9.0 | 7.7 |
| ITO−PHT−P−F | 4.7 | 4.4 |
| ITO−F−ZnP−PHT | 7.1 | 7.0 |
| ITO−PHT−ZnP−F | 10.5 | 6.5 |

[a] F refers to fullerene and P to porphyrin.

The improved model (Scheme 1) describes the charge movements inside the layers more accurately and fits better to the experimental data than the earlier presented model.[37] The values obtained for the quantum yields and charge recombination rate constants (Table 3) are of the same order of magnitude as in the previous work,[37] since in both cases the analysis of slow recombination of photoinduced charge separation is based on the same experimental data. In the improved model, the charge recombination is described by two steps, including rate constants $k_2$ and $k_3$, while in the simplified model[37] it was a single-step process from the state which now can be considered as a combination of $CS_1$ and $CS_2$. Since $k_2 > k_3$ for three first film structures in Table 3, one can conclude that the $CS_2$ state is lower in energy than the $CS_1$ state. For the fourth film, $k_2 < k_3$, suggesting a higher energy for the $CS_2$ state than for the $CS_1$ state. Furthermore, according to the rate constants in Table 3, one can state that bilayers based on zinc porphyrins are more sensitive to the order of the layers in the system. The exact nature of the states $CS_1$ and $CS_2$ is not totally clear. Rather than two well specified states, they should be understood as two different sets of states, each having comparable properties and energies.

## 4. Conclusions

A polythiophene−porphyrin−fullerene triad film was prepared by combining the porphyrin−fullerene dyad and PHT LB monolayers. The photovoltage measurements showed that the photoinduced charge transfer in the porphyrin−fullerene dyad is extended by the secondary ET from PHT to the porphyrin radical cation when a PHT monolayer is deposited in contact with the porphyrin moieties. The photocurrent action spectra indicate that the charge separation in the bilayer is initiated by the primary intralayer electron transfer from the excited porphyrin to the fullerene. The following secondary interlayer ET from the PHT to the porphyrin cation forms the final charge separated state where the negative charges are in the fullerene sublayer and the positive charges are in the PHT layer. According to the proposed kinetic model, the interlayer ET takes place with yield close to unity. Furthermore, the final charge separation has a lifetime of approximately 0.5 s. The lateral charge diffusion in the donor cation and acceptor anion sublayers in the triad LB film prolonged the charge recombination time to hundreds of milliseconds compared to that of 400 ps observed for the intramolecular charge separation in DHD6ee in solutions.[43] The results are promising when considering PHT as a

potential hole transport layer in a molecular solar cell application.

**Acknowledgment.** This work was supported by the Academy of Finland, Project "New Artificial Donor-Acceptor Materials", and the National Technology Agency of Finland.

## References and Notes

(1) Eckert, J.-F.; Nicoud, J.-F.; Nierengarten, J.-F.; Liu, S.-G.; Echegoyen, L.; Barigelletti, F.; Armaroli, N.; Ouali, L.; Krasnikov, V.; Hadziioannou, G. *J. Am. Chem. Soc*. **2000**, *122*, 7467−7479.

(2) Peeters, E.; van Hal, P. A.; Knol, J.; Brabec, C. J.; Sariciftci, N. S.; Hummelen, J. C.; Janssen, R. A. J. *J. Phys. Chem. B* **2000**, *104*, 10174−10190.

(3) Bonhôte, P.; Moser, J.-E.; Humphry-Baker, R.; Vlachopoulos, N.; Zakeeruddin, S. M.; Walder, L.; Grätzel, M. *J. Am. Chem. Soc*. **1999**, *121*, 1324−1336,

(4) Luo, H.; Fujitsuka, M.; Araki, Y.; Ito, O.; Padmawar, P.; Chiang, L. Y. *J. Phys. Chem. B* **2003**, *107*, 9312−9318.

(5) Uosaki, K.; Kondo, T.; Zhang, X.-Q.; Yanigida, M. *J. Am. Chem. Soc*. **1997**, *119*, 8367−8368.

(6) Imahori, H.; Norieda, H.; Yamada, H.; Nishimura, Y.; Yamazaki, I.; Sakata, Y.; Fukuzumi, S. *J. Am. Chem. Soc.* **2001**, *123*, 100−110.

(7) Yamada, H.; Imahori, H.; Nishimura, Y.; Yamazaki, I.; Ahn, T. K.; Kim, S. K.; Kim, D. Fukuzumi, S. *J. Am. Chem. Soc.* **2003**, *125*, 9129−9139.

(8) Imahori, H.; Kimura, M.; Hosomizu, K.; Fukuzumi, S. *J. Photochem. Photobiol., A* **2004**, *166*, 57−62.

(9) Okamoto, K.; Fukuzumi, S. *J. Phys. Chem. B* **2005**, *109*, 7713−7723.

(10) Zeng, H.-P.; Wang, T.; Sandanayaka, A. S. D.; Araki, Y.; Ito, O. *J. Phys. Chem. A* **2005**, *109*, 4713−4720.

(11) Oviedo, J. J.; de la Cruz, P.; Garín, J.; Orduna, J.; Langa, F. *Tetrahedron Lett*. **2005**, *46*, 4781−4784.

(12) Vehmanen, V.; Tkachenko, N. V.; Imahori, H.; Fukuzumi, S.; Lemmetyinen, H. *Spectrochim. Acta, Part A* **2001**, *57*, 2229−2244.

(13) Kesti, T. J.; Tkachenko, N. V.; Vehmanen, V.; Yamada, H.; Imahori, H.; Fukuzumi, S.; Lemmetyinen, H. *J. Am. Chem. Soc.* **2002**, *124*, 8067−8077.

(14) Vehmanen, V.; Tkachenko, N. V.; Efimov, A.; Damlin, P.; Ivaska, A.; Lemmetyinen, H. *J. Phys. Chem. A* **2002**, *106*, 8029−8038.

(15) Vail, S. A.; Tomé, J. P. C.; Krawczuk, P. J.; Dourandin, A.; Shafirovich, V.; Cavaleiro, J. A. S.; Schuster, D. I. *J. Phys. Org. Chem*. **2004**, *17*, 814−818.

(16) Hasobe, T.; Kamat, P. V.; Absalom, M. A.; Kashiwagi, Y.; Sly, J.; Crossley, M. J.; Hosomizu, K.; Imahori, H.; Fukuzumi, S. *J. Phys. Chem. B* **2004**, *108*, 12865−12872.

(17) Guldi, D. M.; Zilbermann, I.; Gouloumis, A.; Vázquez, P.; Torres, T. *J. Phys. Chem. B* **2004**, *108*, 18485−18494.

(18) Galili, T.; Regev, A.; Levanon, H.; Schuster, D. I.; Guldi, D. M. *J. Phys. Chem. A* **2004**, *108*, 10632−10639.

(19) Imahori, H.; Yamada, H.; Nishimura, Y.; Yamazaki, I.; Sakata, Y. *J. Phys. Chem. B* **2000**, *104*, 2099−2108.

(20) Isosomppi, M.; Tkachenko, N. V.; Efimov, A.; Lemmetyinen, H. *J. Phys. Chem. A* **2005**, *109*, 4881−4890.

(21) Ikemoto, J.; Takimiya, K.; Aso, Y.; Otsubo, T.; Fujitsuka, M.; Ito, O. *Org. Lett*. **2002**, *4*, 309−311.

(22) Kodis, G.; Liddell, P. A.; de la Garza, L.; Moore, A. L.; Moore, T. A.; Gust, D. *J. Mater. Chem*. **2002**, *12*, 2100−2108.

(23) Kodis, G.; Liddell, P. A.; Moore, A. L.; Moore, T. A.; Gust, D. *J. Phys. Org. Chem*. **2004**, *17*, 724−734.

(24) Kuciauskas, D.; Liddell, P. A.; Lin, S.; Stone, S. G.; Moore, A. L.; Moore, T. A.; Gust, D. *J. Phys. Chem. B* **2000**, *104*, 4307−4321.

(25) Liddell, P. A.; Kodis, G.; Kuciauskas, D.; Andréansson, J.; Moore, A. L.; Moore, T. A.; Gust, D. *Phys. Chem. Chem. Phys.* **2004**, *6*, 5509−5515.

(26) Otsubo, T.; Aso, Y.; Takimiya, K. *J. Mater. Chem*. **2002**, *12*, 2565−2575.

(27) Sandanayaka, A. S. D.; Ikeshita, K.; Araki, Y.; Kihara, N.; Furusho, Y.; Takata, T.; Ito, O. *J. Mater. Chem*. **2005**, *15*, 2276−2287.

(28) Bell, T. D. M.; Jolliffe, K. A.; Ghiggino, K. P.; Oliver, A. M.; Shephard, M. J.; Langford, S. J.; Paddon-Row: M. N. *J. Am. Chem. Soc*. **2000**, *122*, 10661−10666.

(29) Guldi, D. M.; Imahori, H.; Tamaki, K.; Kashiwagi, Y.; Yamada, H.; Sakata, Y.; Fukuzumi, S. *J. Phys. Chem. A* **2004**, *108*, 541−548.

(30) Tkachenko, N. V.; Tauber, A. Y.; Hynninen, P. H.; Sharonov, A. Y.; Lemmetyinen, H. *J. Phys. Chem. A* **1999**, *103*, 3657−3665.

(31) Tkachenko, N. V.; Vuorimaa, E.; Kesti, T.; Alekseev, A. S.; Tauber, A. Y.; Hynninen, P. H.; Lemmetyinen, H. *J. Phys. Chem. B* **2000**, *104*, 6371−6379.

(32) Tkachenko, N. V.; Vehmanen, V.; Efimov, A.; Alekseev, A. S.; Lemmetyinen, H. *J. Porphyrins Phthalocyanines* **2003**, *7*, 255−263.

(33) Vuorinen, T.; Kaunisto, K.; Tkachenko, N. V.; Efimov, A.; Lemmetyinen, H.; Alekseev, A. S.; Hosomizu, K.; Imahori, H. *Langmuir* **2005**, *21*, 5383−5390.

(34) Guldi, D. M.; Zilbermann, I.; Anderson, G. A.; Kordatos, K.; Prato, M.; Tafuro, R.; Valli, L. *J. Mater. Chem.* **2004**, *14*, 303−309.

(35) Conoci, S.; Guldi, D. M.; Nardis, S.; Paolesse, R.; Kordatos, K.; Prato, M.; Ricciardi, G.; Vicente, M. G. H.; Zilbermann, I.; Valli, L. *Chem.—Eur. J.* **2004**, *10*, 6523−6530.

(36) Chukharev, V.; Vuorinen, T.; Efimov, A.; Tkachenko, N. V.; Kimura, M.; Fukuzumi, S.; Imahori, H.; Lemmetyinen, H. *Langmuir* **2005**, *21*, 6385−6391.

(37) Vuorinen, T.; Kaunisto, K.; Tkachenko, N. V.; Efimov, A.; Lemmetyinen, H. *J. Photochem. Photobiol., A* **2006**, *178*, 185−191.

(38) Alekseev, A. S.; Tkachenko, N. V.; Tauber, A. Y.; Hynninen, P. H.; Osterbacka, R.; Stubb, H.; Lemmetyinen, H. *Chem. Phys*. **2002**, *275*, 243−251.

(39) Efimov, A.; Vainiotalo, P.; Tkachenko, N. V.; Lemmetyinen, H. *J. Porphyrins Phthalocyanines* **2003**, *7*, 610−616.

(40) *Langmuir−Blodgett Films*; Roberts, G., Ed.; Plenum Press: New York, 1990.

(41) Tkachenko, N. V.; Hynninen, P. H.; Lemmetyinen, H. *Chem. Phys. Lett.* **1996**, *261*, 234−240.

(42) Watanabe, I.; Hong, K.; Rubner, M. F. *Langmuir* **1990**, *6*, 1164−1172.

(43) Chukharev, V.; Tkachenko, N. V.; Efimov, A.; Guldi, D. M.; Hirsch, A.; Scheloske, M.; Lemmetyinen, H. *J. Phys. Chem. B* **2004**, *108*, 16377−16385.

(44) Sakomura, M.; Fujihira, M. *J. Photochem. Photobiol., A* **2004**, *166*, 45−56.